

# Multi-slice Behavioral Model of RF Systems and Devices

Aaron Walker, Michael Steer, Kevin Gard, and Khaled Gharaibeh

Department of Electrical and Computer Engineering

North Carolina State University

Raleigh, NC 27695-7914 USA

email: alwalke3@ncsu.edu mbs@ncsu.edu kggard@ncsu.edu kmgharai@ncsu.edu

**Abstract**—System level behavioral modelling is a powerful tool in the RF and microwave designer’s toolbox that allows design tradeoffs to be explored early in a project. Typical models however, have limitations in the frequency range and power levels at which they are applicable and in many instances they fail to capture memory effects that lead to asymmetrical intermodulation behavior observed in the actual system. Here we present a behavioral model with memory that can be extracted from device measurements or simulation results. It uses modular slices to capture the system behavior including asymmetrical intermodulation. The model can be used in system analysis and in harmonic balance or transient circuit simulators.

## I. INTRODUCTION

An RF module can be described as a bandpass nonlinear system as shown in Fig. 1. One of the difficulties in system-level modelling is capturing the behavior of the internal processes that contribute to an observable external frequency response. In particular, the third-order intermodulation distortion products arising from multi-tone stimulus have been traced to several different phenomena, [1] – [5]. Since the contribution of these processes cannot be measured individually, test methods must be used to extract the individual components produced by each source. In a multi-slice model, we choose to represent each source of an output frequency band as a separate slice. In this manner, each nonlinear process with and without memory effects can be modelled separately with the total contribution in a particular frequency band being the phasor sum of the contributions of all slices. In the following work we present results of a two-slice model, Fig. 2, that captures the broadband frequency response of an amplifier as well as the third-order intermodulation (IM3) asymmetry that results with increasing power in a two-tone test.

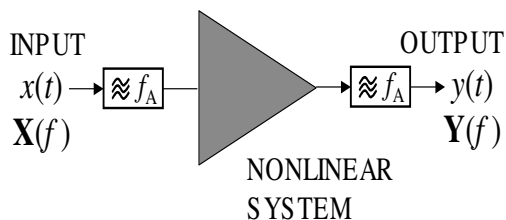


Fig. 1. A unilateral bandpass nonlinear system.

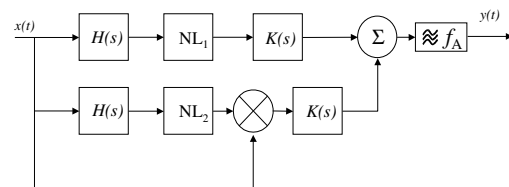


Fig. 2. A two slice nonlinear system behavioral model with passband modelling.

## II. MULTI-SLICE MODELLING METHODOLOGY

The multi-slice modelling approach combines aspects of several different modelling techniques as well as concepts resulting from empirical results. As depicted in Fig. 2, each slice of the model employs the Weiner-Hammerstein architecture that assumes the nonlinear functions to be memory-less with the system frequency response represented by the pre- and post-linear networks,  $H(s)$  and  $K(s)$ . For simplicity, the nonlinear functions are polynomials with real coefficients. The first slice captures the odd-order contributions to the fundamental and the IM3 while the second slice captures the IM3 asymmetry due to second-order effects. An ideal mixer in the second slice translates the baseband frequencies to the passband to accomplish this. The parameters of each component of the model are extracted from a combination of AM-AM and two-tone measurements. In this work the model has been simplified to include only two slices although in general, additional slices can be added to capture other system behavior such as higher order intermodulation distortion (IMD) terms, thermal effects, and harmonic production.

### A. Linear Networks

Since the nonlinear functions are assumed to be memory-less, the linear network frequency responses must be extracted prior to estimating the nonlinear function parameters. The basic assumption in this modelling effort is that all of the broadband memory effects can be captured by the linear networks. The extraction technique used to determine these networks attempts to associate them with actual input and output linear networks present in the system such as the matching and bias circuits. This is in contrast to other models where the networks are extracted in a self-consistent manner

to ensure that the model tracks the frequency response of the measured system.

The extraction procedure is performed from measurements taken at small-signal input powers where there are no IM3 asymmetries and the effect of nonlinear terms above third order are insignificant. With no asymmetries, only the first slice of the model is used for the extraction since it captures the fundamental output response and the IM3 response at small-signal. The two-tone stimulus used in the measurements have 100 kHz separation so the theoretical model of the IM3 components considers that the input stimulus and the IM3 products are all at the same frequency. Under these conditions, the steady-state model output under single tone stimulus is,

$$v_{f_1, \text{out}} = \hat{a}_1 v_{\text{in}} |H(\omega)| |K(\omega)| \quad (1)$$

and the IM3 products are given by

$$v_{\text{IM3}, \text{out}} = \frac{3}{4} \hat{a}_3 v_{\text{in}, \omega_1}^2 v_{\text{in}, \omega_2} |H(\omega)|^3 |K(\omega)|. \quad (2)$$

Here the terms  $\hat{a}_i$  are the real polynomial coefficients for the nonlinear functions, which are unknown at this time. By considering the fundamental and the IM3 products as occurring at the same frequency, a simple ratio of the predicted responses allows computation of  $H(\omega)$  in the frequency domain:

$$\frac{v_{\text{IM3}, \text{out}}}{v_{f_1, \text{out}}} = \frac{\frac{3}{4} \hat{a}_3 v_{\text{in}, \omega_1}^2 v_{\text{in}, \omega_2} |H(\omega)|^3 |K(\omega)|}{\hat{a}_1 v_{\text{in}, \omega_1} |H(\omega)| |K(\omega)|}. \quad (3)$$

With input tones in the two-tone case having equal amplitudes this reduces to

$$\frac{v_{\text{IM3}, \text{out}}}{v_{f_1, \text{out}}} = \frac{3}{4} \frac{\hat{a}_3}{\hat{a}_1} v_{\text{in}, \omega_1}^2 |H(\omega)|^2. \quad (4)$$

Now since  $H(\omega)$  is the only frequency dependent term we can normalize (4) along the frequency axis with respect to the maximum value of the ratio such that  $H(\omega)$  has unity gain at one point in its frequency response.

With the leading linear network frequency response captured, the trailing network frequency response can now be obtained. Starting with the expression for the fundamental output tone, (1), the leading linear network response is divided out yielding

$$\frac{v_{f_1, \text{out}}}{|H(\omega)|} = \hat{a}_1 v_{\text{in}, \omega} |K(\omega)|. \quad (5)$$

Again we can take the trailing linear system as having a lossless response at its maximum magnitude since this only introduces an unimportant constant that shifts the magnitude of the linear network response. The linear gain coefficient of the nonlinearity will incorporate the linear network losses.

### B. Nonlinear Blocks

Once the linear network responses have been extracted the nonlinear functions can be estimated. The extraction method for the two slices in this model differ since they capture different system behavior.

The first slice nonlinearity produces the broadband fundamental output for all power levels and the system IM3 response

under small-signal conditions. The nonlinearity is modelled by an odd-order polynomial by using a modified fit to the AM-AM data. The modification uses information from the two-tone small-signal response to produce a better fit to the IM3 response at small input powers. The coefficients are real since using AM-PM data for complex coefficient extraction would require knowing the phase of the IM3 products in the model development which cannot be measured at present. Output from this slice at the IM3 tones is given by,

$$y_{\text{IM3}, 1} = \sum_{n=3}^N \sum_{l=0}^{\frac{n-3}{2}} a_{n,l} v_{\text{in}}^n |H(\omega)|^n |K(\omega)| \quad (6)$$

where  $N$  is the order of the polynomial and  $a_{n,l}$  is the modified memory-less polynomial coefficient  $\hat{a}_n$ ,

$$a_{n,l} = \frac{\hat{a}_n}{2^{n-1}} \binom{n}{\frac{n-3}{2} - l, l+1, l, \frac{n+1}{2} - l}. \quad (7)$$

The second slice nonlinearity produces the IM3 asymmetry seen in measured data with increasing input power. The odd-order polynomial in the first slice cannot produce this effect since each of the IM3 tones is generated by the same coefficients. Physical understanding of the IM3 asymmetry suggests that this phenomena is a result of differences in the baseband impedance at positive and negative envelope frequencies, [2]. It has been established in [6], that the IM3 components and the fundamental have the same phase for the weakly nonlinear region of a system. This suggests that to first order the IM3 asymmetry can be attributed to an expansion term for one of the tones and a compression term for the other as if the baseband contribution to the IM3 tones has an in-phase and an 180° component. As to which IM3 component contains the expansion and which the compression, the second-slice model considers the following baseband contributions to IM3.

For a second-order nonlinearity, the baseband component generated at  $\omega_1 - \omega_2$  can be translated to the IM3 tones by mixing with the fundamentals as shown in Fig. 2 and given at steady state by

$$v_{bb} = \hat{a}_2 v_{\text{in}}^2 |H(\omega)|^2 \cos(\omega_1 - \omega_2)t \quad (8)$$

$$v_{\text{IM3L}, bb} = \hat{a}_2 v_{\text{in}}^3 |H(\omega)|^2 |K(\omega)| \cos(2\omega_1 - \omega_2)t \quad (9)$$

$$v_{\text{IM3H}, bb} = \hat{a}_2 v_{\text{in}}^3 |H(\omega)|^2 |K(\omega)| \cos(\omega_1 - 2\omega_2)t. \quad (10)$$

As (9) and (10) show, the baseband components upconverted to the IM3 tones are at positive and negative frequencies thus resulting in a difference in sign in their combination with the contribution of the first slice. A similar derivation can be applied to higher order terms in an even order polynomial representation of the second-slice nonlinearity. From this derivation, the coefficients for an even-order polynomial can be fit to the difference between the measured IM3 tones. The output of the second slice is then combined with that of the first slice with opposite sign for each of the IM3 products such that the asymmetry is reproduced.

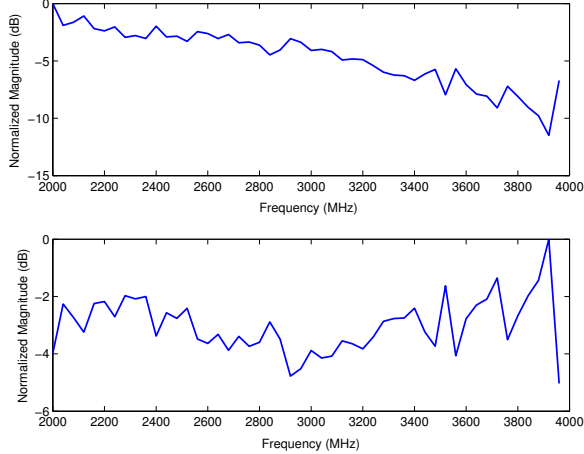


Fig. 3. Extracted pre-filter and post-filter frequency responses.

### III. EXPERIMENTAL RESULTS

The model extraction techniques presented above were applied to measurements taken on the LNA portion of the RFMD 2486 LNA+mixer IC. This device is intended for PCS applications and has an operational bandwidth from 1.5 – 2.5 GHz. Data was taken over 2-4 GHz, which allowed modelling both inband and out-of-band performance. Power levels of the stimulus were swept from  $-15$  to  $-1$  dBm. The two-tone measurements were taken with tones of equal power and constant frequency separation (100 kHz) as the tones were swept across the frequency band.

The frequency response of the linear networks in the multi-slice model were computed from the  $-15$  dBm input power point using AM-AM and IM3 measurements as in (4) and (5). As shown in Fig. 3, the pre-filter response has 10 dB of attenuation over the octave frequency band, while the post-filter response is flatter over this range. The large variation in the magnitude response at higher frequencies is a function of the IM3 measurements at small-signal levels. The IM3 distortion at these frequencies was near the noise floor of the spectrum analyzer used in the experiment and the collected data shows the expected variation in amplitude. As a consequence of this variation, the fit of the measured data at higher frequencies is degraded since the pre-filter response is raised to the power of the nonlinearity in each of the slices.

Without the high frequency variation, it can be seen that the majority of the frequency response of the system is due to the pre-filter. From the expression for the first slice output, the effect of the attenuation in the pre-filter is magnified by the nonlinearity so that the attenuation in the IM3 products is significantly higher, Fig. 4.

The ability of the multi-slice model to track the measured fundamental output is shown in Fig. 5. Here the model output at three different input powers shows the excellent agreement with the measured data across the entire frequency span except at the highest input power where the polynomial fit to the measured data was less accurate.

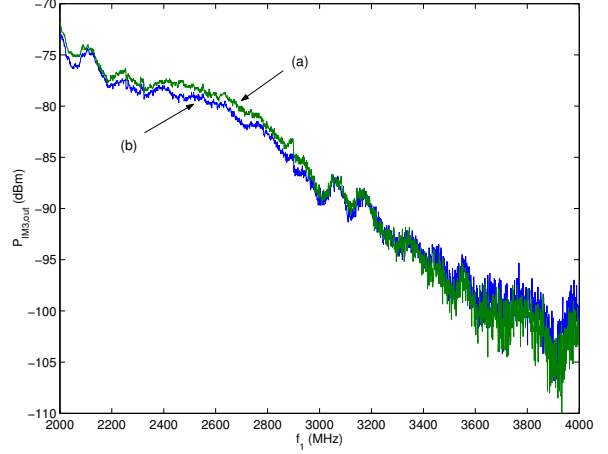


Fig. 4. Measured output power of (a) IM3H and (b) IM3L at  $-15$  dBm input tone power.

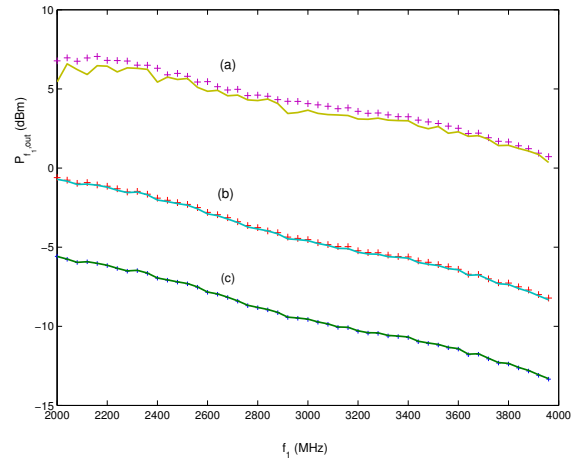


Fig. 5. Measured (+) and modelled (line) fundamental output power at (a)  $-1$  dBm, (b)  $-10$  dBm, and (c)  $-15$  dBm input tone power.

The model also predicts the IM3 asymmetry seen at higher input powers as shown in Figs. 6 and 7. Here the deviations between the model and the measured response reside mainly at the higher frequencies where measurement noise impacted the linear system extraction.

Plotting the IM3 measured and modelled data versus input power and input voltage shows that the model predicts the asymmetry well up to an input power of  $-6$  dBm with large differences above this level (Figs. 8 and 9). The deviations result from the inability of the polynomial model in the first slice to accurately reproduce saturation effects in the IM3 products.

### IV. CONCLUSION

Results from applying the multi-slice behavioral model methodology and extraction procedures have been presented. This simple model using only magnitude information and established measurement procedures can predict fundamental

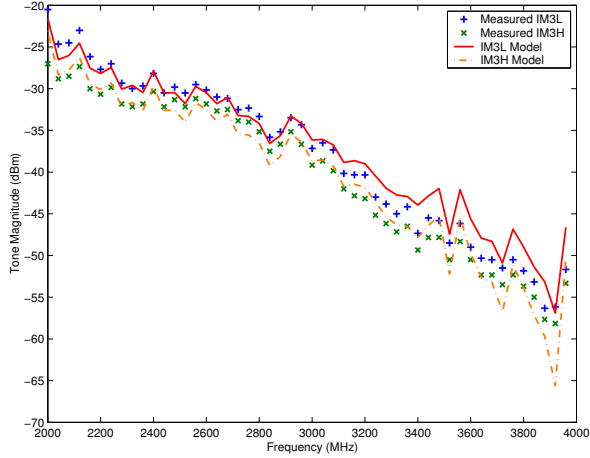


Fig. 6. IM3 modelled and measured frequency response at  $-7$  dBm.

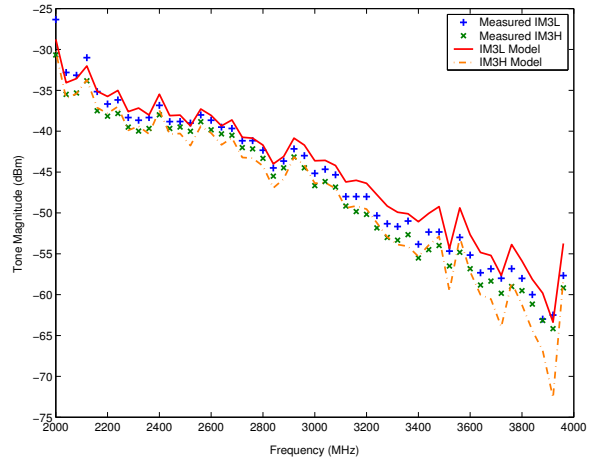


Fig. 7. IM3 modelled and measured frequency response at  $-9$  dBm.

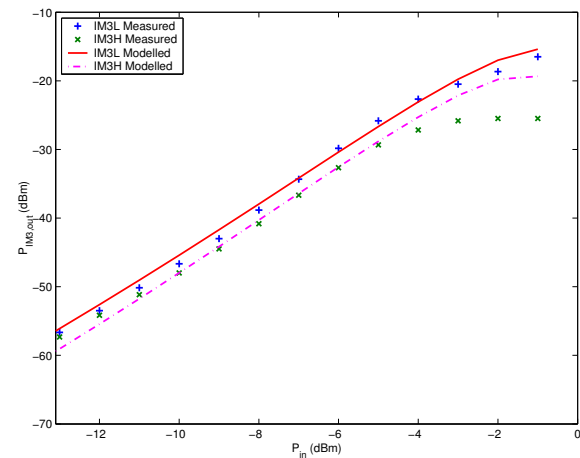


Fig. 8. IM3 modelled and measured response at 3 GHz,  $P_{out}$  vs.  $P_{in}$ .

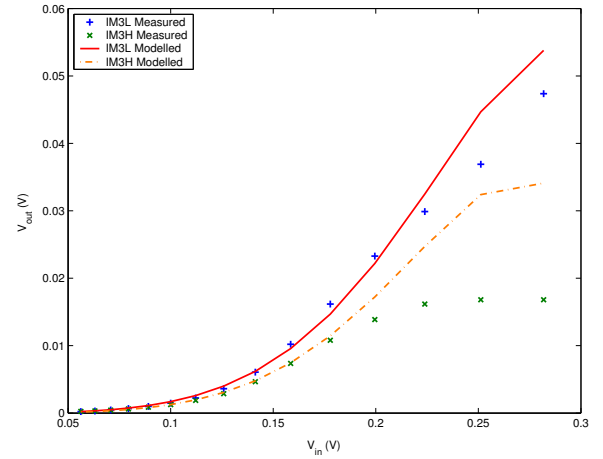


Fig. 9. IM3 modelled and measured response at 3 GHz,  $V_{out}$  vs.  $V_{in}$

output and IM3 asymmetries over a broad frequency range and power level of the input stimulus. Improvements to the model can be achieved by utilizing a more robust extraction technique for the linear networks, acquiring phase information of the IM3 to better describe the phasor addition of the contributors to intermodulation distortion, and expanding the baseband model to include effects of varying the tone separation. The flexibility of the multi-slice architecture has been demonstrated in the reproduction of a single phenomena that a traditional AM-AM, AM-PM model cannot predict, thus one can envisage additional slices in a more complex model to capture other effects such as thermal memory effects and out-of-band emissions. One of the most important attributes of the architecture of the behavioral model is that it can be used in harmonic balance and transient circuit simulators as well as in system analysis.

## REFERENCES

- [1] R. S. Tucker, "Third-order Intermodulation Distortion and Gain Compression in GaAs FET's," *IEEE Trans. on Microwave Theory and Techn.*, vol. MTT-27, pp. 400-408, May 1979.
- [2] J. F. Sevic, K. L. Burger, and M. B. Steer, "A Novel Envelope-termination Load-pull Method for ACPR Optimization of RF/Microwave Power Amplifiers," in 1998 MTT-S Int. Microwave Symp. Dig., vol. 2, pp. 723-726, June 1998.
- [3] J. H. K. Vuolevi, T. Rahkonen, and J. P. A. Manninen, "Measurement Technique for Characterizing Memory Effects in RF Power Amplifiers," *IEEE Trans. on Microwave Theory and Techn.*, vol. 49, pp. 1383-1389, Aug. 2001.
- [4] N. B. de Carvalho and J. C. Pedro, "A Comprehensive Explanation of Distortion Sideband Asymmetries," *IEEE Trans. on Microwave Theory and Techn.*, vol. 50, pp. 2090-2101, Sept. 2002.
- [5] H. Ku and J. S. Kenney, "Behavioral Modeling of Nonlinear RF Power Amplifiers Considering Memory Effects," *IEEE Trans. on Microwave Theory and Techn.*, vol. 51, pp. 2495-2504, Dec. 2003.
- [6] N. Suematsu, Y. Iyama, and O. Ishida, "Transfer Characteristic of IM3 Relative Phase for a GaAs FET Amplifier," *IEEE Trans. on Microwave Theory and Techn.*, vol. 45, pp. 2509-2514, Dec. 1997.